Development of Integrated Transport Analysis Suite for LHD Plasmas Towards Transport Model Validation and Increased Predictability*)

Masayuki YOKOYAMA, Chihiro SUZUKI, Ryosuke SEKI, Masaki OSAKABE, Mikiro YOSHINUMA, Masahiko SATO, Arimitsu WAKASA[1)], Sadayoshi MURAKAMI[1)], Atsushi FUKUYAMA[1)], Yasuhiro SUZUKI, Katsumi IDA, Hyungho LEE[2)] and LHD Experiment Group

National Institute for Fusion Science, Toki 509-5292, Japan
[1)]*Department of Nuclear Engineering, Kyoto University, Kyoto 606-8501, Japan*
[2)]*National Fusion Research Institute, Daejeon 305-806, Korea*

(Received 27 November 2012 / Accepted 31 January 2013)

In this study, the integrated transport analysis suite, TASK3D-a, was developed to enhance the physics understanding and accurate discussion of the Large Helical Device (LHD) experiment toward facilitating transport model validation. Steady-state and dynamic (transient) transport analyses of NBI (neutral-beam-injection)-heated LHD plasmas have been greatly facilitated by this suite. This will increase the predictability of the transport properties of LHD plasmas toward reactor-relevant regimes and reactor-scale plasmas.

Keywords: integrated transport analysis suite, TASK3D-a, LHD, NBI plasma, slowing-down effect, energy balance analysis

DOI: 10.1585/pfr.8.2403016

1. Introduction

The LHD plasma parameter regimes, such as those of density, temperature and long-pulse operation, have been successfully extended [1]. The energy confinement property has been analyzed mainly on physics-topics basis, such as high-electron [2], high-ion temperature [3], and medium-to-high density plasmas [4] by comparing the radial profiles (one-dimensional, 1D) of the experimental and neoclassical energy fluxes. On the other hand, the unified energy confinement scaling law for helical plasmas was deduced as ISS95 [5] and its extension ISS04 [6], which consider the global (zero-dimensional, 0D) energy confinement time. Extending the physics understanding of the energy confinement beyond a scaling law (0D) is mandatory for increasing the predictability for further enhancement of plasma performance in the present experiment and designing a fusion-reactor scenario such as FFHR-d1 [7]. For this purpose, an integrated transport analysis suite, TASK3D-a (analysis version), was developed to accelerate the energy balance analysis involving the radial (1D) profiles measured in the LHD. This paper describes the calculation procedure of TASK3D-a, and its various features.

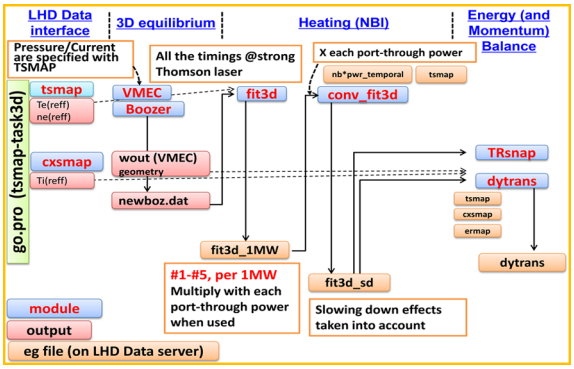

Fig. 1 Calculation procedure employed in TASK3D-a01. Blue, red and orange boxes indicate module (computation program), output files, and eg format files, respectively.

2. Calculation Procedure of TASK3D-a

The calculation procedure employed in TASK3D-a ("a01" as the first version) is schematically summarized in Fig. 1. It consists of four parts; LHD data interface, three-domensional (3D) equilibrium, heating (only NBI at this moment), and energy (and momentum) balance analysis.

2.1 LHD data interface part

The LHD data interface is based on the real-time coordinate mapping system, TSMAP [8], in which the radial coordinate is transformed from the real coordinate (major radius, R) to the effective minor radius (r_{eff}) by searching

author's e-mail: yokoyama@LHD.nifs.ac.jp
*) This article is based on the presentation at the 22nd International Toki Conference (ITC22).

for the "best-fit" equilibrium in a pre-calculated VMEC [9] database (VMEC-DB). Here, the "best-fit" is meant to satisfy the in-out symmetry (with respect to the magnetic axis position at approximately the peak of the electron temperature, T_e) of the measured T_e profile. On the basis of the coordinate mapping, T_e and density profiles are provided as functions of r_{eff}, and ion temperature (T_i) profile as well when it is available (through "cxsmap").

2.2 3D equilibrium part

The 3D equilibrium component re-evaluates the VMEC equilibrium (fixed-boundary calculation) for all timings of strong Thomson lasers (for T_e measurement) by implementing parameters for the pressure and current profiles of a "best-fit" TSMAP at each time slice. Note the following remarks on the VMEC re-evaluation:

- Last closed flux surface (R_{mn} and Z_{mn}): This is taken from the VMEC-DB corresponding to a_{99} defined by the "best-fit" TSMAP. Here, a_{99} is the minor radius in which 99% of the total stored energy is confined. Because a_{99} is defined on the basis of experimentally observed profiles, it is not always the same as the minor radius in the VMEC-DB (say, a_{DB}), which is based on given pressure and current profiles.
- Pressure profile: p_0 (the peak value) and p_f (the peaking factor) are taken from the "best-fit" TSMAP. These two values provide the functional form of pressure. If a_{99} differs from a_{DB}, the flux label $\psi = (r/a_{99})^2$ is used as an approximation instead of $\psi = (r/a_{DB})^2$.
- Current profile: The measured value of the total current is provided. The profile is assumed to be proportional to 1-ψ^2.
- Total toroidal magnetic flux: This is provided by *phiedge0*$*(a_{99}/a_{DB})^2$, where *phiedge0* is the toroidal flux for a vacuum case in the VMEC-DB. If *phiedge0* and a_{DB} do not exist in the VMEC-DB, interpolation is performed using the available data.

In Fig. 2, an example is shown of the comparison between the "best-fit" TSMAP ($a_{99} \sim 0.62$ m) and VMEC-DB ($a_{DB} \sim 0.63$ m) for a particular shot-timing. The value "p_TSMAP" is given as the input of VMEC2000. The approximation, $\psi = (r/a_{99})^2 \sim \psi = (r/a_{DB})^2$, has little impact on the mapping between r_{eff} (TSMAP), $< r >$(VMEC calc.) and R. The module, Boozer, maps the VMEC coordinates to the Boozer coordinates.

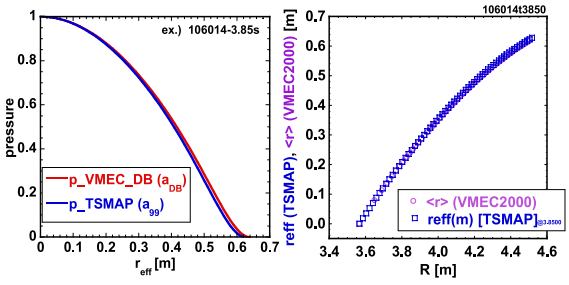

Fig. 2 Comparison of "best-fit" TSMAP and VMEC-DB for a particular shot-timing (3.85 s of the shot 106014).

Because the "best-fit" TSMAP is defined by only satisfying "T_e peak to the magnetic axis" and "in-out symmetry", it does not necessarily reproduce all the equilibrium properties well. Thus, this approach should be considered to be only one of the practical approaches for providing equilibrium for experimental analysis. The "*wout*" file produced by the VMEC can be replaced by that based on another equilibrium reconstruction approach to observe or investigate the impact of equilibrium on the analyses.

2.3 Heating part

The heating component currently includes only the NBI module. The "fit3d" has been developed to evaluate the radial profiles of the NBI absorbed power, beam pressure, beam source and induced momentum [10]. The calculation consists of the following three parts.

- HFREYA: calculations of the birth profile (from the generation of the beam particles in the beam source to ionization in the plasma)
- MCNBI: birth-ions are followed (shorter than the energy slowing-down (SD) time, but longer than the orbit effects such as prompt loss can be reflected)
- Steady-state solution of the Fokker-Planck equation is obtained without considering orbit effects.

Note that T_i is not always measured for selected timings. Thus, $T_i = T_e$ is assumed for standard use of TASK3D-a01, because the effect of T_i on the deposition properties is known to be rather small. The results are stored in the "*eg*" file format on the Kaiseki Data Server for the LHD experiment [11].

The "conv_fit3d" has been developed [12] to evaluate the NBI absorbed power and induced momentum by considering the beam SD effect, on the basis of the results obtained by "fit3d" (which does not include the SD effect). The calculation method employed in "conv_fit3d" is explained here. It is assumed that ions with injection energy, E_{inj}, are produced with a typical time interval Δt = 100 ms (corresponding to the interval of the selected timings in the "fit3d" calculations, which is currently the interval between timings with strong Thomson laser intensity for fine T_e profile measurement) during NBI injection. This time interval is comparable with the typical SD time of injected beam ions (estimated as $\geqslant$ a hundred of ms, and also as lately seen in Fig. 4) in plasmas with density of low-10^{19} m^{-3} and T_e of a few keV. Of course, the time interval should be smaller to increase the accuracy, depending on the availability of a fine T_e profile measurement. These ions are followed until their energy becomes zero. The heating power is evaluated for contributions from ions with the energy above T_i (equal to T_e). Then, the SD process for ions with E_{beam} at each timing is evaluated. Below,

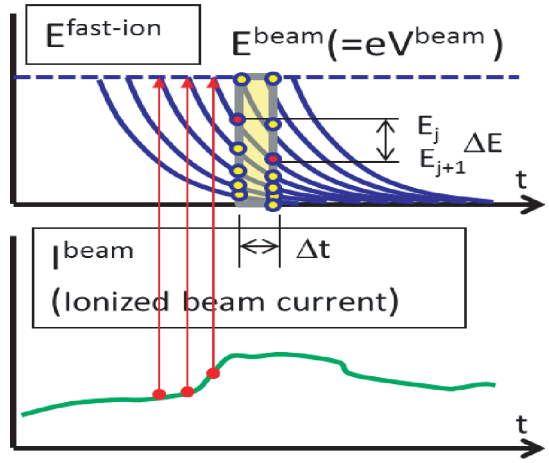

Fig. 3 Schematic explanation on considerations of SD effect in NBI deposition calculations by "conv_fit3d".

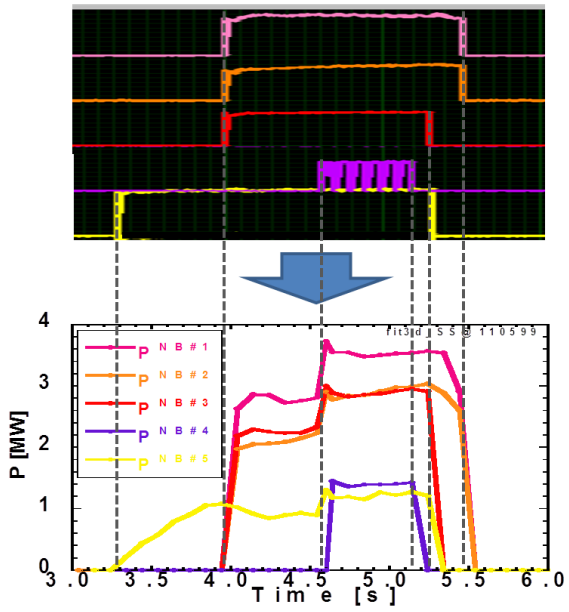

Fig. 4 Time evolution of NBI absorbed power with SD effect compared with the injection wave-form in a particular discharge, 110599. #1 to #5 and their associated colors correspond to beam lines.

the subscript j indicates the ions injected at the "j-th" previous time-step before t_i. Thus, the ion energy injected at $t = t_i$ is expressed as $E_{i,0}$(equal to E_{beam}). Similarly, the ion energy expressed as $E_{i,j}$ at $t = t_i$ is denoted by $E_{i+1,j+1}$ at the next timing, $t = t_{i+1}$. The relationship between $E_{i,j}$ at $t = t_i$ and that at the next time-step, deduced from

$$E_{i+1,j+1} = \left[E_{i,j}^{3/2} \exp\left(-\frac{3\Delta t}{\tau_{se}}\right) - E_c^{3/2}\left\{1 - \exp\left(-\frac{3\Delta t}{\tau_{se}}\right)\right\}\right]^{2/3} \quad (1)$$

where E_C is the critical energy of the beam ions at which the Coulomb friction of the bulk electrons and ions become equal, and τ_{se} is the velocity SD time due to the electron drag. The heating power within one time-step is calculated as the sum of $\Delta E_{i,j} = E_{i,j} - E_{i+1,j+1}$ by weighting the ionized beam current $I_{i,j}^{beam}$. This evaluation process is shown schematically in Fig. 3.

A particular example, shot 110599, is shown in Fig. 4, in which a carbon pellet was injected at $t \sim 4.55$ s. The #5 beam-line was injected from $t = 3.3$ s, and beam-lines #1, #2 and #3 were injected from $t = 4.0$ s, followed by #4 from $t = 4.6$ s (modulated for charge-exchange spectroscopic measurement). The figure shows that the gradual increase (decay) in the absorbed power after injection is turned-on (turned-off) is appropriately evaluated. Note that the "conv_fit3d" calculation continues until 1.0 s after each beam is turned-off by default. The abrupt increase in the absorbed power is also clearly evaluated, which is of great importance for grasping the heating efficiency increase of a carbon pellet injection shown in a recent ion-temperature parameter expansion experiment in the LHD [13].

Note that time-dependent GNET (GNET-TD [14]) calculations have become available, although they are time-consuming. A benchmarking comparison of the SD process evaluation in the approach combining "fit3d" and "conv_fit3d" described here and that of GNET-TD will be performed in the near future.

2.4 Energy balance analysis part

The energy balance analysis part consists of two modules, "TRsnap" [15] (for steady-state analysis) and "dytrans" [16] (for so-called dynamic transport). "TRsnap" has been modified on the basis of TASK/TR (a module of TASK [17]). The power input from NBI (from either "fit3d" (steady state NBI input) or "conv_fit3d" (SD effect considered) and the collisional energy transfer are considered in the energy balance analysis. Other terms such as radiation loss and charge-exchange loss, which require the TASK3D-a extension for edge-plasma physics, have been ignored. Furthermore, "dytrans" evaluates the energy flows due to the temporal variation in the plasma profiles in addition to the steady-state energy flow. Thus, the temporal behavior of the energy confinement properties of transient plasmas can be analyzed, for identifying when confinement improvement occurs as an example. One such example is shown in Fig. 5, where the temporal change in the density-normalized energy flux of ion (Q_i/n_i) is plotted as a function of the T_i gradient close to the mid-radius ($r_{eff}/a_{99} \sim 0.3$) of a particular shot (110599). The slope connecting each data point and the origin, $(Q_i/n_i)/(-dT_i/dr_{eff})$, corresponds to the "steady-state" diffusivity of the ion energy. This figure shows that the T_i gradient increases (more than three times) from pellet injection (at ~4.60 s) with a smaller (less than twice) increase in Q_i/n_i until 4.76 s at which the central T_i reaches its maximum value during the shot. This trajectory indicates the evolution of confinement improvement. The T_i gradient subsequently decreases with little change in Q_i/n_i. In the context of this paper, all the points plotted in Fig. 5 can be prepared

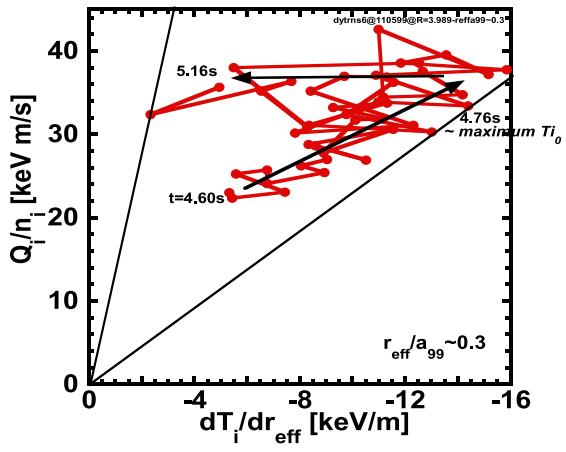

Fig. 5 Time evolution of density-normalized energy flux of ion as a function of ion-temperature gradient close to mid-radius ($r_{\rm eff}/a_{99}$ 0.3) of a particular shot (110599).

by a single execution of TASK3D-a. In this way, analyses of energy confinement properties of LHD plasmas can be significantly accelerated by using TASK3D-a, which will be of great help for deepening the physics understanding.

3. Flexibility and Coming Extension of TASK3D-a

TASK3D-a employs a flexible structure that allows by module/file replacement, improvement, and inclusion of new modules to be performed relatively easily. One example is the replacement of the "*wout*" file produced by the VMEC. Since "*wout*" is a standard VMEC output file, the equilibrium obtained by other approaches such as STELLOPT equilibrium reconstruction [18] can be implemented in the "*wout*" file in Fig. 1 instead of that obtained from TSMAP in order to investigate the impact of equilibrium specification on energy balance analysis.

In the coming extension (from "a01" to "a02", and then the following version of TASK3D-a), the ECH and ICH modules (LHDGauss [19] and TASK/WM [17], respectively) will be implemented so that the overall heating scenario in the LHD can be systematically examined. The multi-ion-species effect will also be implemented using the effective ion charge $Z_{\rm eff}$ [20] and carbon density profile as a function of $r_{\rm eff}$ whenever available. The carbon density profile is of significant interest for analyzing impurity-hole phenomena [21] in a combination of SD-considered NBI absorbed power. Edge-plasma characteristics such as neutral particle penetration and charge exchange with plasma particles are also part of the coming extensions in combination with appropriate numerical codes and databases. The inclusion of neoclassical energy and particle flux calculations will make it possible to accelerate the comparison between the so-called experimental and neoclassical energy fluxes to elucidate "anomalous" contribution to the energy flux systematically in a wide range of LHD plasmas.

4. Conclusion and Future Prospects

The development of the integrated transport analysis suite, TASK3D-a, for LHD experiments has progressed. It is now possible to conduct energy balance analyses (steady-state/dynamic) for NBI-heated LHD plasmas in a much faster time scale than before. The temporal change in the confinement state has been relatively easily analyzed using this suite to provide valuable information such as when the confinement improvement occurs. The coming extensions will increase the functionality of the suit, and are expected to facilitate transport model validation against the LHD experiment, thus increasing the predictive capability toward higher-performance LHD plasmas and reactor-scale plasmas.

Finally it should be mentioned that TASK3D-a is open to collaborators and an English manual has been prepared [22].

Acknowledgments

This study has been supported by the NIFS Collaborative Research Programs NIFS11KNTT008 and a grant-in-aid from the Future Energy Research Association.

[1] O. Kaneko *et al.*, OV/2-1, presented at 24th IAEA Fusion Energy Conference (San Diego, Oct. 2012).
[2] K. Ida *et al.*, Phys. Rev. Lett. **91**, 085003 (2003).
[3] K. Nagaoka *et al.*, Nucl. Fusion **51**, 083022 (2011).
[4] A. Dinklage *et al.*, EX/P3-14, presented at 24th IAEA Fusion Energy Conference (San Diego, Oct. 2012).
[5] U. Stroth *et al.*, Nucl. Fusion **36**, 1063 (1996).
[6] H. Yamada *et al.*, Nucl. Fusion **45**, 1684 (2005).
[7] A. Sagara *et al.*, Fusion Eng. Des. **87**, 594 (2012).
[8] C. Suzuki *et al.*, Plasma Phys. Control. Fusion **55**, 014016 (2013).
[9] S.P. Hirshman and J.C. Whitson, Phys. Fluids **26**, 3353 (1986), and at http://vmecwiki.pppl.wikispaces.net/VMEC
[10] S. Murakami *et al.*, Trans. Fusion Technol. **27**, 256 (1995).
[11] M. Emoto *et al.*, Fusion Eng. Des. **81**, 2019 (2006).
[12] M. Osakabe (National Institute for Fusion Science), private communication (2012).
[13] H. Takahashi *et al.*, EX/2-5, presented at 24th IAEA Fusion Energy Conference (San Diego, Oct. 2012).
[14] H. Yamaguchi, S. Murakami *et al.*, P3-18, presented at 22nd International Toki Conference (2012).
[15] R. Seki *et al.*, Plasma Fusion Res. **6**, 2402081 (2011).
[16] H. Lee, K. Ida *et al.*, Plasma Phys. Control. Fusion **55**, 014011 (2013).
[17] A. Fukuyama, http://bpsi.nucleng.kyoto-u.ac.jp/task/
[18] N. Pablant (Princeton Plasma Physics Laboratory, USA), private communication (2012).
[19] S. Kubo *et al.*, Proc. 11th International Congress on Plasma Physics, Sydney, AIP Conf. Proc. **669**, 187 (Jul. 2002).
[20] H. Zhou, S. Morita *et al.*, Rev. Sci. Instrum. **81**, 10D706 (2010).
[21] M. Yoshinuma *et al.*, Nucl. Fusion **49**, 062002 (2009).
[22] M. Yokoyama for TASK3D Users and Developers, NIFS-MEMO-61, National Institute for Fusion Science, Nov. 2012.